HIGH-RESOLUTION IRON-LINE SPECTROSCOPY

R.E. GRIFFITHS

Harvard-Smithsonian Center for Astrophysics

Cambridge, Massachusetts 02138

ABSTRACT

Methods of resolving the iron lines, the most common X-ray emission lines in both galactic and extragalactic X-ray sources, are briefly reviewed. A self-focussing crystal spectrometer is shown to be the most suitable instrument, and the optimum crystal geometry is spherical (Schnopper and Taylor 1980). The principles of operation of such a spherical crystal imaging spectrometer (SCIS) are briefly reviewed, and its sensitivity is shown to be two orders of magnitude better than a focal plane crystal spectrometer on AXAF. A Spacelab version of this payload would be very cost-effective.

Introduction

The emphasis in this paper will be on high-resolution spectroscopy (the X-ray astronomer's definition: $\frac{E}{\Delta E} > 100$) of the iron lines in the 6-7 keV range. The first, and generally the strongest lines detected in proportional counter spectra of both galactic and extragalactic X-ray sources have been the iron lines in the 6-7 keV range. The reason for this line strength in optically thin plasmas is twofold: a) the high relative abundance of iron; and b) the ionization balance of elements at the temperatures typical of X-ray sources, i.e., 10^7 -10^8 K. Figure 1 is plotted from the tabulations of Raymond and Smith (1978) and shows theoretical calculations of the relative emissivities of the strongest iron lines between 3.10^7 and 10^8 K (not including satellite lines) and illustrates the reason that the Fe XXV/XXVI complex is so dominant in X-ray spectra - other elements are largely stripped out at lower temperatures. In particular, the effective temperature of intracluster gas in galaxy clusters, typically 8 x 10^7 K (see Mushotzky et al. 1978), is such that the iron complex forms the most useful diagnostic of cluster parameters.

The most common line observed in binary X-ray sources is the fluorescent iron line, for reasons of high fluorescence yield (a factor of 10 higher than any other element - see Table 1, taken from Pravdo 1978), coupled with the high relative abundance.

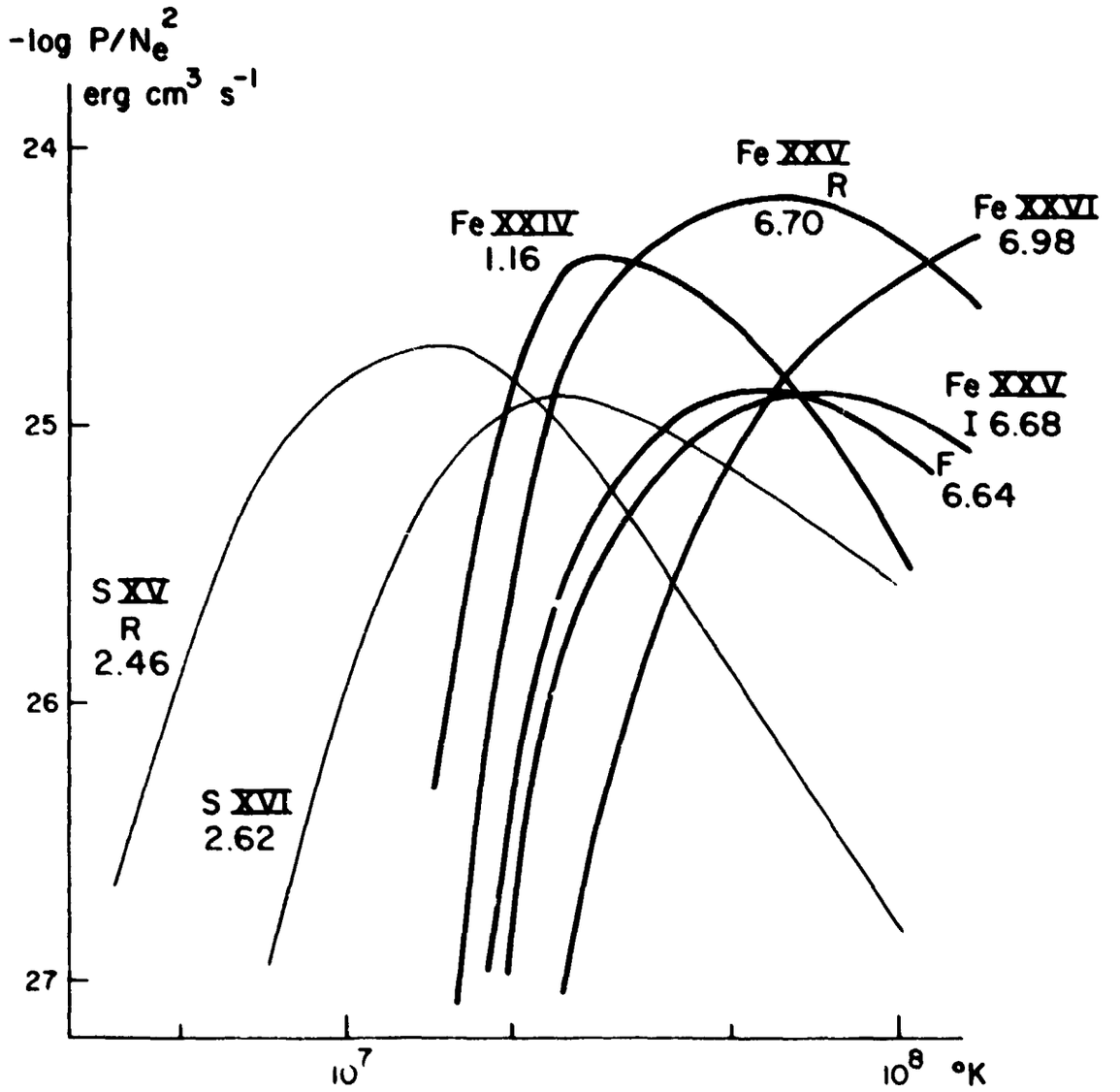

Figure 1 Relative emissivities of the strongest iron lines in a low-density plasma at temperatures between 3.10^7 and 10^8 K (not including satellite lines).

TABLE 1

FLUORESCENCE EMISSION

Element	Relative Abundance	Fluor. Yield	Kα Energy	Rel. Equiv. Width (dN/dE^{-1})
Si	$3. \times 10^{-5}$	0.04	1.74	0.03
S	1.6×10^{-5}	0.08	2.31	0.03
Ar	$8. \times 10^{-6}$	0.13	2.96	0.03
Ca	$2. \times 10^{-6}$	0.16	3.69	0.01
Fe	$4. \times 10^{-5}$	0.35	6.40	1.00
Ni	$2. \times 10^{-6}$	0.41	7.47	0.07

Table 1 Relative fluorescence emission-line strengths (from Pravdo 1978)

Dispersive Versus Non-Dispersive Spectroscopy

How can the iron line energy be reached for spectroscopy, and how can the iron lines be resolved for measurements of temperature, abundance, density and ionization balance?

Figure 2 illustrates the resolution typical of energy-dispersive devices (dashed lines) and those of dispersive devices (solid lines). Non-dispersive devices have been used almost exclusively thus far in the measurements of iron line strengths at 6-7 keV, but have insufficient resolution to separate the lines of Fe XXV from Fe XXVI. Gas proportional scintillation counters have twice the resolving power of the conventional gas proportional counters, but this is still insufficient to clearly separate Fe XXV from XXVI, or to resolve the Fe XXV triplet lines (note that lines of FE XXV, $1s^2$-1s2p and $1s^2$-1snp were recently resolved by a GPSC in the spectrum of Cas A - Andreser et al. 1981). The solid-state detector, of the kind flown on HEAO-2, (Holt, 1976), does have the resolution to separate Fe XXV from XXVI, and so, in principle, does a high-spatial resolution array of solid-state devices, i.e., the charge-coupled device. Considerable progress has been made in the development of a CCD with sufficient depletion depth for the 6 keV range (Griffiths et al. 1981; Peckerar et al. 1981), but solid-state performance equivalent to that from a conventional Si(Li) detector, has yet to be demonstrated from a full CCD array at this energy, although the lowest CCD noise levels are

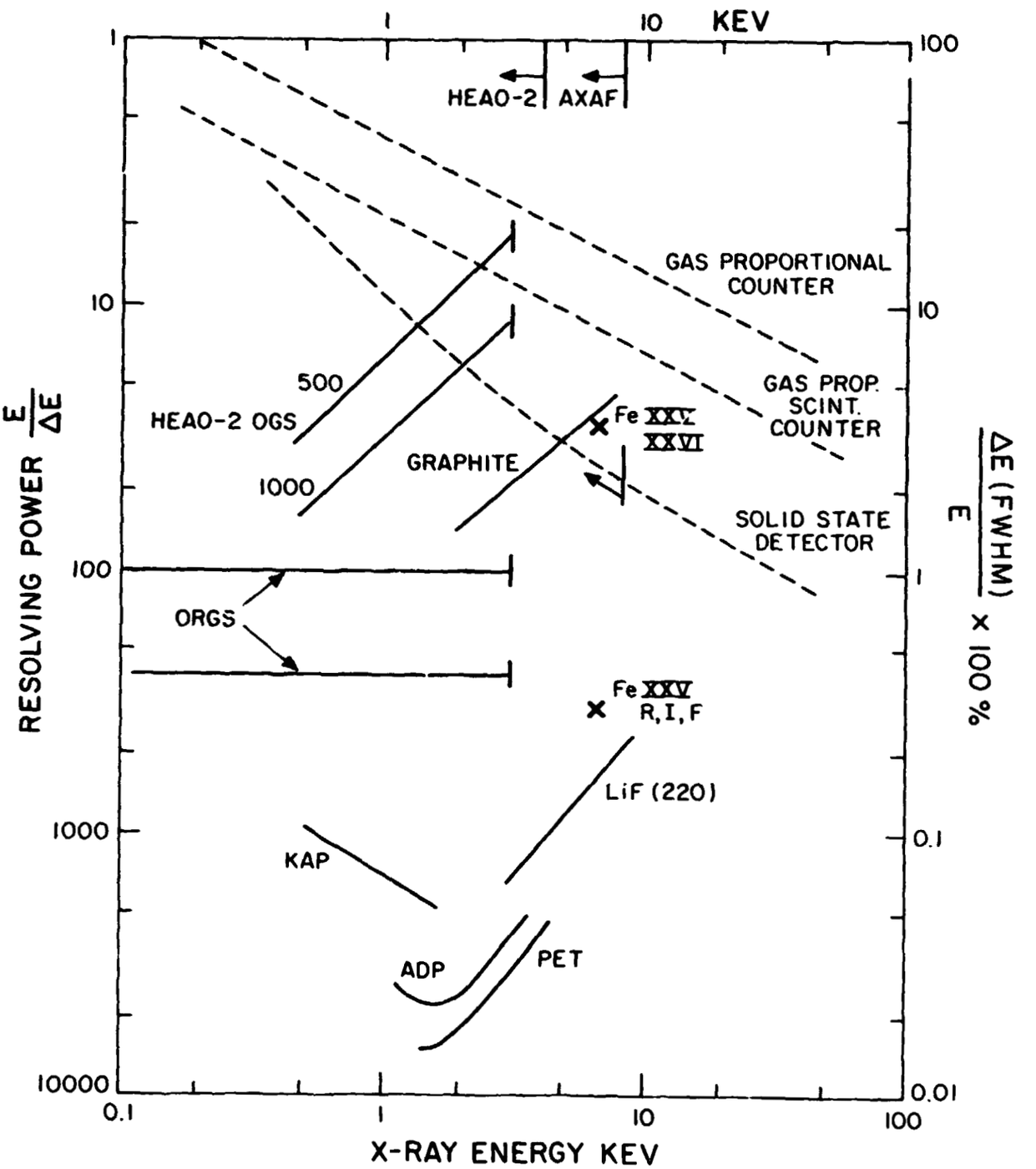

Figure 2 Energy resolution of non-dispersive devices (dashed lines) and dispersive devices (solid lines).

comparable to or below that of the Si(Li) detector output. Both the conventional solid-state detector and the CCD have to rely on grazing-incidence optics for large collection areas, and in the case of HEAO-2, this resulted in no collection area at the 6 keV iron lines. For the proposed mirror design for AXAF, the effective collecting area at 6-7 keV will be about 200 cm^2 (Zombeck 1981).

To separate the Fe XXV triplet lines, the necessary resolving power is about 300, and this can be provided by crystal spectroscopy, lithium fluoride having a suitable 2d spacing (41^c Bragg angle for the atomic planes of LiF 220). In order to achieve high sensitivity, the particle background in the X-ray detector has to be effectively eliminated, so that the spectrometer is photon-limited for a large number of applications. Previous satellite-borne crystal spectrometers, on Ariel V, ANS, OSO-8 have been limited in sensitivity by their particle-induced background levels, concomitant on the flat crystal panels employed in each case. For large crystal areas and small detector sizes, some form of self-focussing is obviously required, and various geometries have been proposed, and some instruments flown, in recent years. The conical-segment spectrometer (Fig. 3a) was first proposed by Woodgate et al. (1973), and needs to be scanned over the required energy range. The convex version of this, described by Berthelsdorf et al. 1976 (Fig. 3b) is energy-dispersive along the detector axis, and has been employed on the solar maximum mission (Rapley et

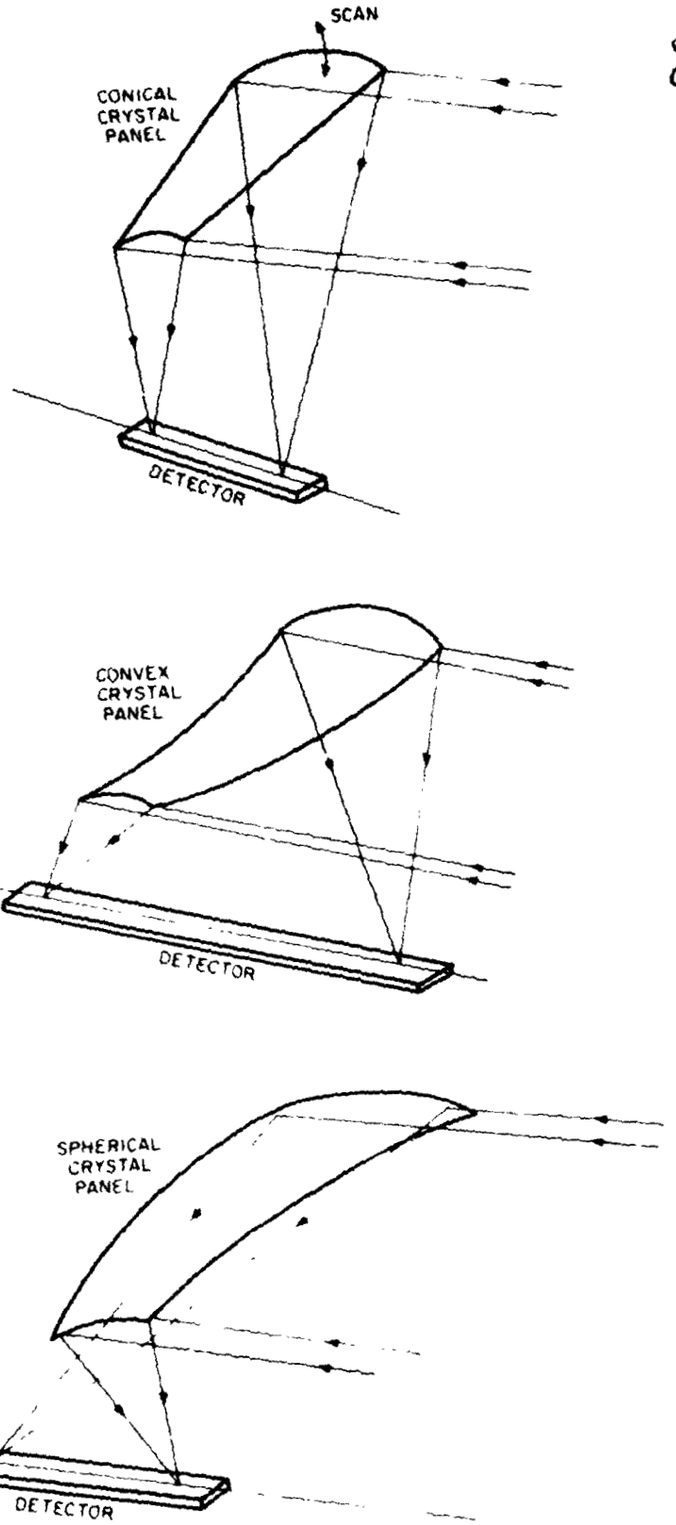

Figure 3 Self-focussing crystal spectrometers: a) conical spectrometer; b) convex spectrometer; and c) spherical spectrometer.

al. 1977, Acton et al. 1981). The latter geometry leads to degraded performance for off-axis or extended sources, however, and the optimum geometry is the spherical case, fully described by Schnopper and Taylor (1981), and shown in Figure 3c. A brief description of the performance of this spectrometer will be repeated here.

Spherical Crystal Imaging Spectrometer

The axis of the spectrometer, along which the X-ray detector lies, is pointed at the target X-ray source. The operation of the instrument can be understood by reference to Figure 4, which shows the principle of operation in more detail. X-rays of energy E_1, incident in a cylindrical sheet on the top of the crystal panel, are focussed onto the detector at the point Z_1, and X-rays of energy E_2, incident in a similar sheet on the bottom of the panel, are focussed on the other end of the detector at Z_2. For a sphere radius of 2.5m, using lithium fluoride for the iron lines, the dispersion along the axis is about 0.4 mm per eV, or 2.4 mm for a 6 eV crystal-limited resolution element. Position sensitivity of 0.5 mm in the proportional detector is therefore sufficient for the energy-dispersive line focus. The position-sensitive detector reads out each X-ray event as it occurs, and the entire spectrum is thus recorded in a parallel fashion, with no mechanical scanning. The total energy range covered by the spectrometer is

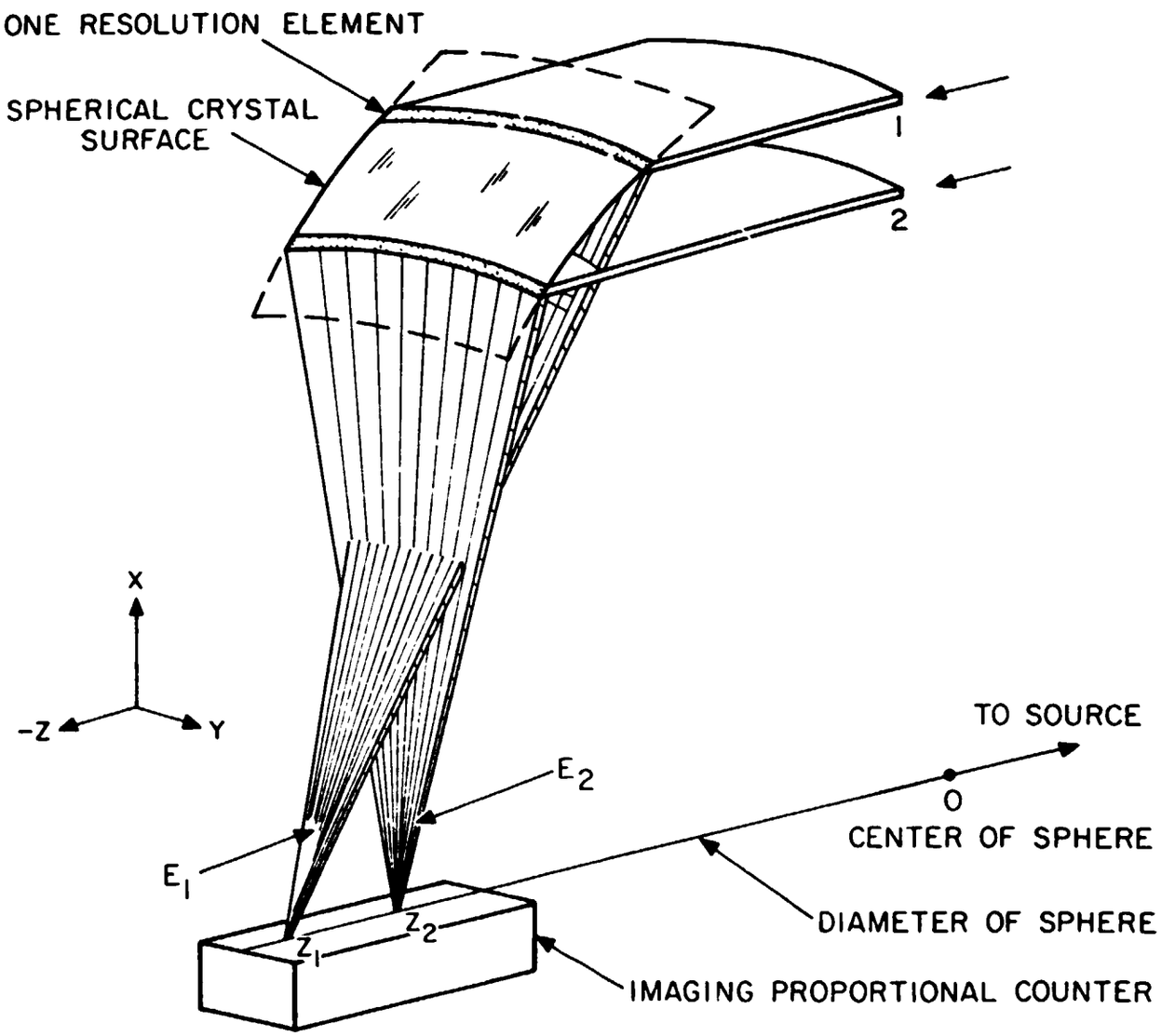

Figure 4 Basic operation of the spherical spectrometer.

determined by the range of Bragg angles for X-rays incident at the extreme ends of the spherical section.

A real, imperfect crystal consists of a mosaic of individual perfect crystal blocks, on a microscopic scale, with a resultant increase in integrated reflectivity (James 1948). For the spherical spectrometer, the rocking curve width of the scanned flat crystal panel becomes a corresponding crystal-limited resolution element along the position-sensitive detector. For a Bragg angle of 45^{c}, the energy resolution in the spherical spectrometer case is the same as that for the scanned flat crystal panel. For Bragg angles much less than 45^{c}, there is some gain in the effective energy resolution with the spherical geometry, but the effective area of the crystal panel is reduced and the geometry does not use the available volume as efficiently as the 45^{c} case.

An extended X-ray source, or a spacecraft attitude error for a point source, will result in some slight degradation in performance, but it can easily be shown that the effects are almost negligible in terms of spectroscopic resolution. These effects are most easily understood by considering spacecraft attitude errors and a point X-ray source. It is obvious that, as the spacecraft and spectrometer rotate slightly around the center of the sphere, the spherical symmetry guarantees that the X-rays will still be focussed on the line joining the center to the X-ray source, with a small change in the energy range of the reflected X-rays. The detector will no longer be exactly on this

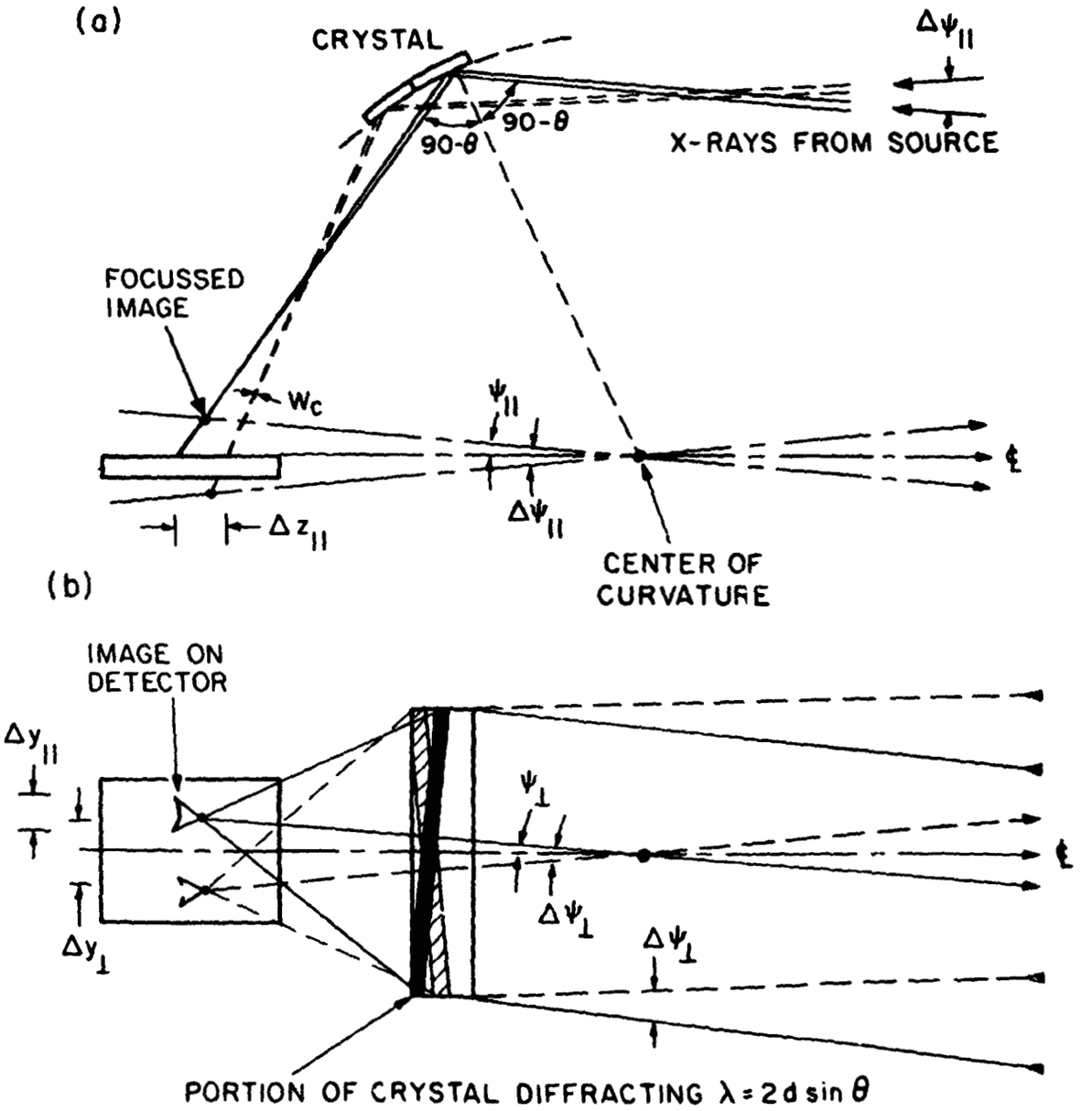

Figure 5 Effect of off-axis X-rays: a) in the plane of dispersion; and b) orthogonal to the plane of dispersion.

line focus, however. It is most instructive to separate the pointing error into two components, one orthogonal to the plane of dispersion (Fig. 5b) and one in the dispersion plane. For the orthogonal pointing error, a stigmatic focus is formed on the detector, along an arc about the center of the sphere, where this arc is displaced in the manner shown (< 1 cm for a $0^{\circ}.5$ pointing error).

A pointing error in the plane of dispersion (Fig. 5a) results in a line focus lying slightly above or below the detector anode, and the image at any particular energy is formed in a hyperbolic arc on the detector, where the curvature of the arc causes an insignificant loss of energy resolution. The post-facto spacecraft or instrument aspect solution can be used to correct for the instantaneous size and position of the hyperbolic arc, so that the resulting spectrum is not significantly degraded. The pointing requirements for the spherical spectrometer are thus minimal, of the order of $\pm 0^{\circ}.1$.

The imaging of an extended source can best be considered in terms of point source components, where each off-axis point source is imaged into a short, hyperbolic arc, as described above. The energy resolution of the spectrometer in the plane of dispersion is slightly degraded by source extent, but this effect becomes important only for sources greater than $0^{\circ}.2$ in diameter, using lithium fluoride panels. In the plane orthogonal to the dispersion plane, the angular resolution is limited by the crystal rocking curve width of about 5 arc minutes.

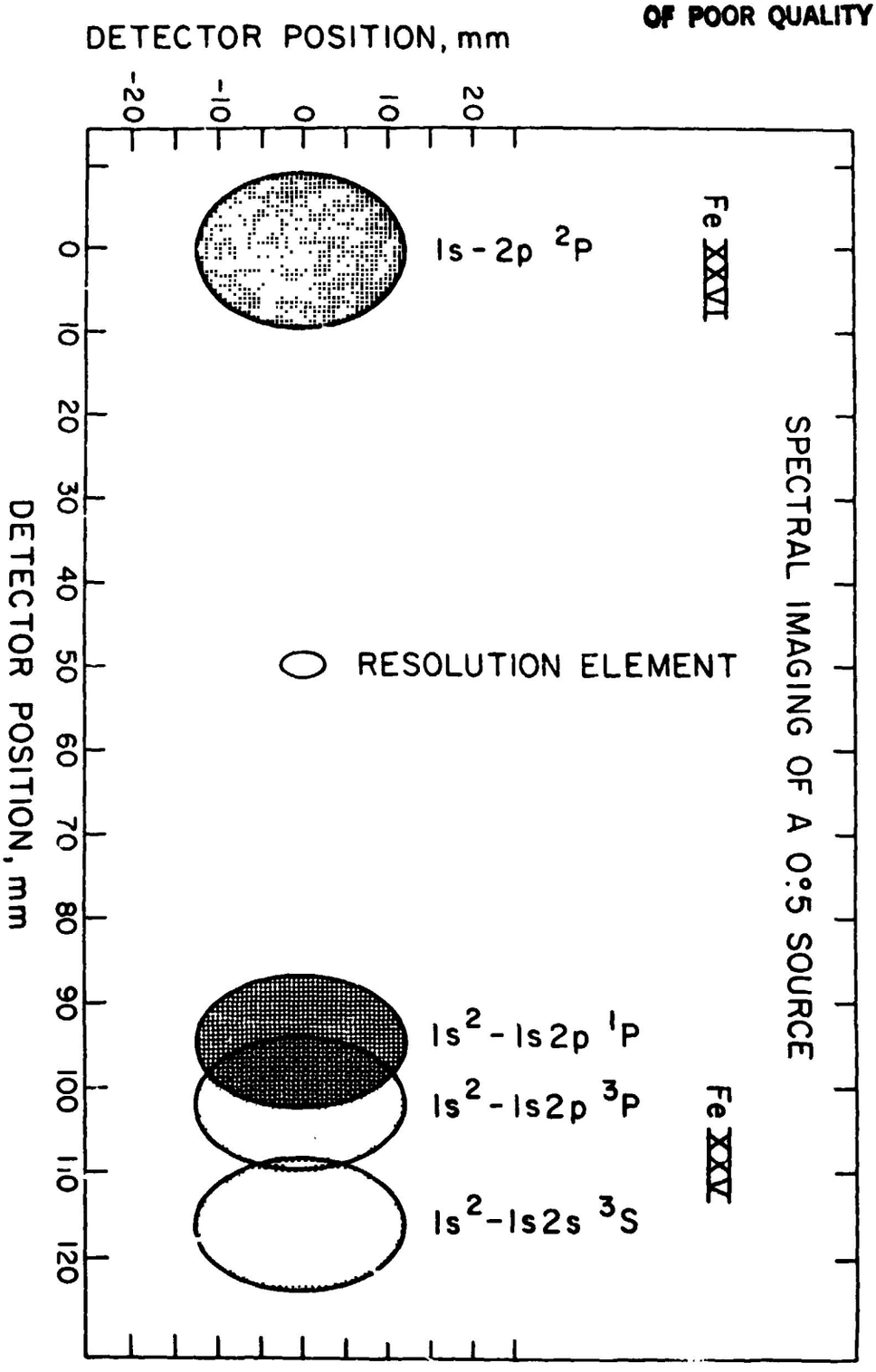

Figure 6 Idealized image of a cluster of galaxies of 0°.5 extent, showing shape of monochromatic images in lines of Fe XXV and XXVI.

Projected SCIS Performance

The combination of spectral and spatial resolution is illustrated in Figure 6, which shows an idealized image of a source about $0^{\circ}.5$ in extent, emitting lines from hydrogen-like and helium-like iron. For this extreme source size (eg., the Virgo cluster), the helium-like triplet is slightly blended but still usefully resolved. The resolution element for a point X-ray source emitting narrow lines is also shown in Figure 6 for comparison purposes, and in this case the helium-like triplet is fully resolved.

The iron spectral features which can be covered by a 4° range in Bragg angle using lithium fluoride are summarized in Table 2, and extend from the neutral FeI absorption edge at 7.1 keV through the Fe XXV and XXVI transitions to a 10% red-shifted Fe XXVI line. The energy resolution of the LiF crystals is 6 eV.

The plasma diagnostics which can be performed with this energy range and resolution are indicated in Table 3, a list of necessary sensitivities and resolving powers for the iron lines, taken from the work of Pahcall and Sarazin (1978). These include the dielectronic satellite lines of helium-like iron, which may be at comparable fluxes to lines of the more usual transitions. Generally, it can be seen from the table that the resolving power of the crystal spectrometer described here is necessary for these plasma diagnostics.

TABLE 2

IRON SPECTRAL FEATURES

Fe I K abs. edge	7.13 keV
Fe I Kβ	7.05
Fe XXVI 1s-2p	6.93
Fe XXV 1s ^{2}-1s2p	6.70
1s ^{2}-1s2p $^3P_2$	6.66
1s ^{2}-1s2s ^3S	6.64
Fe I Kα_1	6.39
Fe XXVI 10% redshifted	6.30

Table 2 Iron spectral features in the 6-7 keV range

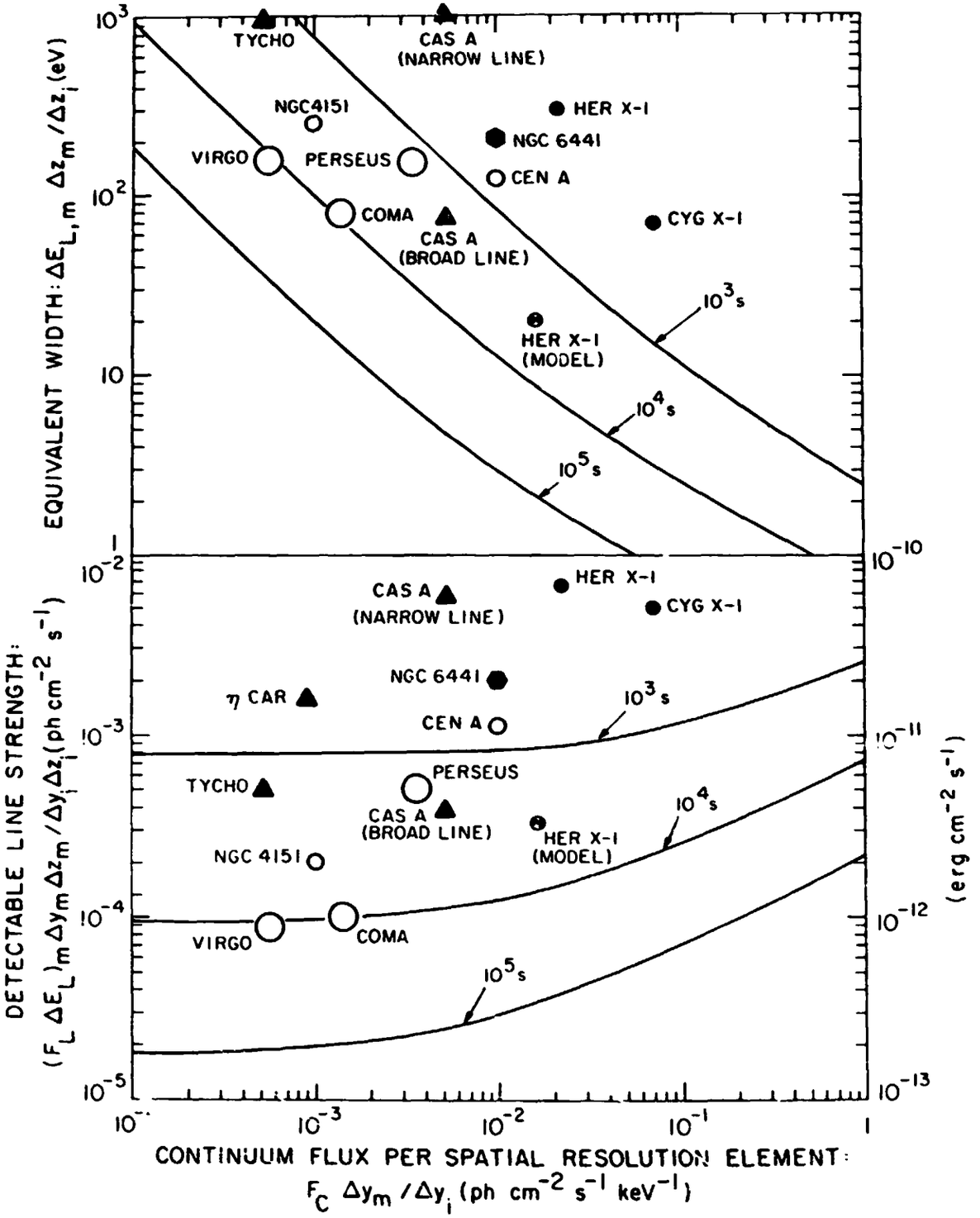

Figure 7 Minimum detectable equivalent widths and line strengths.

The spherical crystal imaging spectrometer achieves high sensitivity by employing a large crystal area and a large concentration factor into a low background detector (the concentration factor is about 100, relative to the flat crystal case). The minimum detectable equivalent widths and line strengths, for an instrument with 0.4 m^2 projected area, are shown in Figure 7, which demonstrates that these senstivities are a function of continuum flux for the stronger sources, but the spectrometer is photon-limited, i.e., limited by line count statistics, for most sources of interest in observation times of $\sim 10^4$s. With longer observation times, $\sim 10^5$s or longer, the instrument sensitivity becomes limited by detector background. Figure 7 also indicates some of the line strengths and equivalent widths of iron line features already detected by proportional counters on rocket and satellite experiments. In these cases where the source is extended, the observed strengths are shown per spatial-spectral resolution element of the proposed instrument (5 arc min^2 x 6 eV). It can be readily seen from these sensitivity curves that the instrument is sensitive to any of the plotted sources in an observation time of 10^4s, and for some, an observation time of only 10^2s is necessary. As an example, the instrument is sensitive, in a 10^4s observation of the Perseus cluster, to features with 30 eV equivalent width, in each resolution element. Such sensitivity is sufficient to measure the basic plasma parameters of temperature, relative abundance for iron, and ionization balance on a

TABLE 3

PLASMA DIAGNOSTICS FOR CLUSTERS
(from Pancall and Sarazin 1978)

		Lines	Temp. Range 10^6 K	Necessary Sensitivity eV	Necessary Resolving Power $E/\Delta E$
	•	Fe XXV F/R	.3-2	40	200
Temperature		XXV $W\alpha/I\beta$	.1-.3	80	85
Determination		XXVII I_λ/I_β	.2-.5	9	190
	•	XXV diel.	.2-1	100	210
	•	XXVI diel.	.4-2	8	210
Relative	•	Fe XXV + XXVI	.2-2	470	2
Abundance	•	XXV	.2-3	13	100
Determination	•	XXVI	.5-5	67	35
	•	Fe XXII inner shell	.1-.3	51	110
	•	XXIII inner shell	.1-.7	20	170
Ionization	•	XXIV inner shell	.1-1	46	340
Balance	•	XXVI/XXV	.2-4	20	85

Table 3 Necessary sensitivities and resolving powers for cluster plasma diagnostics (from Pancall and Sarazin 1978)

spatially-resolved scale of 5 arc min over the extended cluster emission. The Virgo cluster line emission can similarly be detected in each 5 x 5 arc min spatial resolution element in 10^4s, and the combined data from the whole cluster would have a significance of about 15σ.

Line emission from supernova remnants is generally expected to be broadened by the expansion velocity profile, which has been measured in some cases for optical filaments, but not directly for the expanding X-ray shell. For CasA, the expansion may be estimated as ~400 kms^{-1} FWHM, and this expansion is expected to be observable as a broadened iron line covering about 15 resolution elements, with an average significance of about 6σ in each element. The sensitivity in the (unrealistic) non-expansion case and for the case of an expanding shell source are both shown in Figure 7.

In the optically-thick scattering plasma of accretion disks around compact objects, the narrow line emission is severely reduced from the optically-thin case (Felten and Rees 1972; Griffiths 1972). Ross et al. (1978) have modelled the line emission from Her X-1, and the narrow line core predicted by their model is plotted in Figure 8, i.e., the residual line core should be detectable in a 10^4s observation, with sufficient sensitivity to measure the relative strengths of the resonance, intercombination and forbidden lines of Fe XXV, giving a measure of density in the source. These residual line cores are an order of magnitude weaker than in the optically-thin case. Some of the

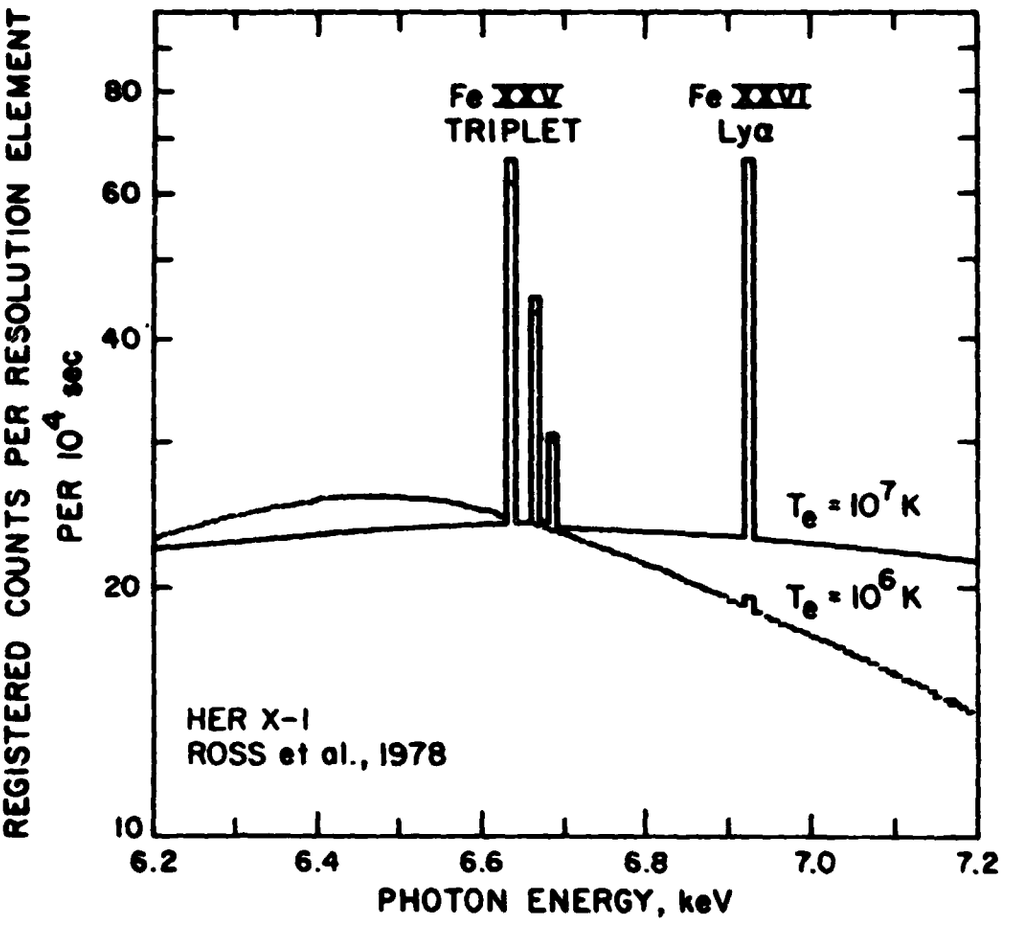

Figure 6 Calculation of counts from a 10^4s observation of Her X-1, using the residual line intensities from the model of Ross et al. 1978.

fluorescence iron lines in binary X-ray sources are expected to be an order of magnitude stronger than these residual Fe XXV lines in Her X-1.

It is noteworthy that the sensitivity of an AXAF focal plane crystal spectrometer (i.e., the LiF crystal) would be about 10^{-2} ph cm^{-2} s^{-1} at the iron lines (Schnopper and Taylor 1981), two orders of magnitude worse than the instrument proposed here. The reason for this difference is simply one of area, with the realization that such spectrometers are photon-limited. The effective area of AXAF at 6.7 keV is between 100 and 200 cm^2, whereas the projected area of the crystal panels in the proposed SCIS is of the order of 10^4 cm^2. Considering high-resolution crystal spectroscopy alone, the use of grazing-incidence optics is clearly inefficient. The same argument remains valid, but to a lesser extent, at lower energies, where the AXAF effective area of ~1000 cm^2 can still be surpassed by a crystal panel with the appropriate atomic spacing for Bragg reflection and concentration of the silicon or sulphur lines, for example.

SCIS - Proposed Payload

The SCIS payload, as proposed for a Spacelab mission by SAO in collaboration with the Saclay group (Schnopper et al. 1978; Schnopper and Taylor 1980), is shown in a cut-away drawing in Figure 9. The large crystal panels are relatively cheap to fabricate, and a total payload cost has been estimated at around $2 million.

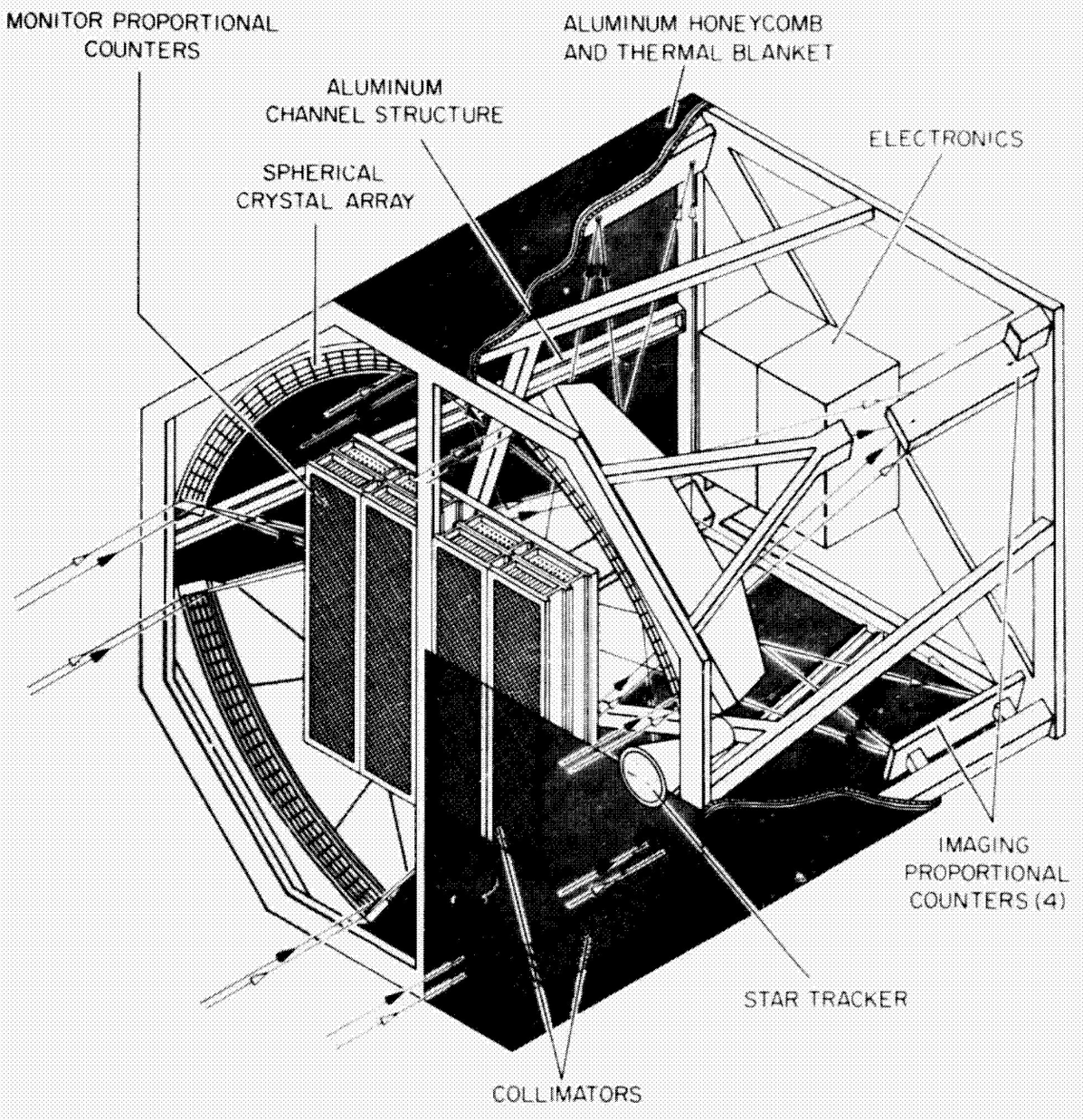

Figure 9 SCIS payload, as proposed for a Spacelab mission (Schnopper et al. 1978).

The large central area is shown here filled with a monitor proportional counter for measurement of the overall spectrum of X-ray sources. A gas scintillation proportional counter would have twice the energy resolution and would better complement the crystal spectrometer. Ideally, the central area would be filled by an efficient grazing incidence collector, covering at least the ~1-8 keV range, with an array of solid-state devices in the focal plane.

Conclusions

The most efficient, and by far the most economical way of performing high-resolution spectroscopy of the 6-7 keV iron lines is by means of a spherical crystal imaging spectrometer. Such an instrument, of Spacelab-pallet proportions, would have a sensitivity two orders of magnitude better than an AXAF focal-plane crystal spectrometer, and would be sensitive in observation times of 10^4s or less, to all of the iron lines detected thus far by proportional counters.

REFERENCES

Acton, L.W. et al. 1980, Solar Phys., 65, 53.

Andresen, R.D., Manzo, G., Peacock, A., Taylor, B.G., Catura, R.C., Culhane, J.L., and Berthelsdorf, R. 1981, Proc. 15th ESLAB Symposium, 'X-ray Astronomy', ESA.

Bahcall, J.N., and Sarazin, C.L. 1977, Ap.J. (Letters), 213, L99.

Bahcall, J.N., and Sarazin, C.L. 1978, Ap.J., 219, 781.

Berthelsdorf, R.F., Mitchell, R.J., and Culhane, J.L. 1976, Space Sci. Instr., 2, 349.

Felten, J.E., Rees, M.J., and Adams, T.F. 1972, Astron. and Astrophys., 21, 139.

Griffiths, R.E. 19 2, Astron. and Astrophys., 21, 97.

Griffiths, R.E., Polucci, G., Mak, A., Murray, S.S., and Schwartz, D.A. 1981, Proc. Soc. Photo-Opt. Instr. Eng. (SPIE), 'Solid-state imagers for astronomy', 290, 62.

Holt, S.S. 1976, Space Sci. Instr., 2, 205.

James, R.W., 1948, 'The Optical Principles of the Diffraction of X-rays', The Crystalline State, Vol. II, G. Bell and Sons, London.

Mushotzky, R.F., Serlemitsos, P.J., Smith, B.W., Boldt, E.A., and Holt, S.S. 1978, Ap.J., 225, 21.

Peckerar, M.C., McCann, D.H., and Yu, L. 1981, Rev. Sci.Instr., in press.

Pravdo, S.H. 1979, Proc. CCSPAR Symposium on X-ray Astronomy,

Advances in Space Exploration (COSPAR), Vol. 3, p169, eds. W.A. Baity and L.E. Peterson.

Rapley, C.G., Culhane, J.L., Acton, L.W., Catura, R.C., Joki, E.G., and Bakke, J.C. 1977, Rev. Sci. Instr., 48, 1123.

Raymond, J.C., and Smith, B.W. 1977, Ap.J. Supp., 35, 419.

Ross, R.R., Weaver, R., and McCray, R. 1978, Ap.J., 219, 292.

Schnopper, H.W., and Taylor, B.C. 1980, App. Opt., 19, 3306.

Schnopper, H.W., Delvaille, J.P., Griffiths, R., Taylor, P.O., Koch-Miramond, L., Bergeron, J., Ilovaisky, S., Montmerle, T., Rocchia, R., and Rothenflug, R., 1978, Proposal to NASA, P 834-10-78.

Schnopper, H.W., and Taylor, B.C. 1981, App. Opt., in press.

Woodgate, B.E., Lowinger, T., and Schneider, M. 1973, Appl. Opt., 12, 2759.

Zombeck, M.V. 1981, Opt. Eng., 20, 297.